Naunyn-Schmiedeberg's Arch Pharmacol (2016) 389:369–379
DOI 10.1007/s00210-015-1205-3

ORIGINAL ARTICLE

Pioglitazone alleviates cardiac and vascular remodelling and improves survival in monocrotaline induced pulmonary arterial hypertension

Arnica Behringer[1] · Manuela Trappiel[2] · Eva Maria Berghausen[1] · Henrik ten Freyhaus[1] · Ernst Wellnhofer[3] · Margarete Odenthal[5] · Florian Blaschke[4] · Fikret Er[6] · Natig Gassanov[6] · Stephan Rosenkranz[1] · Stephan Baldus[1] · Kai Kappert[2] · Evren Caglayan[1]

Received: 20 August 2015 / Accepted: 21 December 2015 / Published online: 7 January 2016

Abstract Pulmonary arterial hypertension (PAH) is a fatal disease with limited therapeutic options. Pathophysiological changes comprise obliterative vascular remodelling of small pulmonary arteries, elevated mean pulmonary arterial systolic pressure (PASP) due to elevated resistance of pulmonary vasculature, adverse right ventricular remodelling, and heart failure. Recent findings also indicate a role of increased inflammation and insulin resistance underlying the development of PAH. We hypothesized that treatment of this condition with the peroxisome proliferator-activated receptor-γ (PPARγ) activator pioglitazone, known to regulate the expression of different genes addressing insulin resistance, inflammatory changes, and vascular remodelling, could be a beneficial approach. PAH was induced in adult rats by a single subcutaneous injection of monocrotaline (MCT). Pioglitazone was administered for 2 weeks starting 3 weeks after MCT-injection. At day 35, hemodynamics, organ weights, and -indices were measured. We performed morphological and molecular characterization of the pulmonary vasculature, including analysis of the degree of muscularization, proliferation rates, and medial wall thickness of the small pulmonary arteries. Furthermore, markers of cardiac injury, collagen content, and cardiomyocyte size were analyzed. Survival rates were monitored throughout the experimental period. Pioglitazone treatment improved survival, reduced PASP, muscularization of small pulmonary arteries, and medial wall thickness. Further, MCT-induced right ventricular hypertrophy and fibrosis were attenuated. This was accompanied with reduced cardiac expression of brain natriuretic peptide, as well as decreased cardiomyocyte size. Finally, pulmonary macrophage content and osteopontin gene expression were attenuated. Based on the beneficial impact of pioglitazone, activation of PPARγ might be a promising treatment option in PAH.

Keywords Pulmonary hypertension · Rat · PPAR · Monocrotaline · Right ventricle

Arnica Behringer, Manuela Trappiel, Kai Kappert and Evren Caglayan contributed equally to this work.

✉ Evren Caglayan
evren.caglayan@uk-koeln.de

[1] Department of Internal Medicine III; Heart Center, University of Cologne, Cologne, Germany

[2] Institute of Laboratory Medicine, Clinical Chemistry and Pathobiochemistry; Center for Cardiovascular Research (CCR), Charité–University Medicine Berlin, Berlin, Germany

[3] Department of Cardiology, German Heart Center Berlin, Berlin, Germany

[4] Department of Cardiology, Charité–University Medicine Berlin, Berlin, Germany

[5] Department of Pathology, University of Cologne, Cologne, Germany

[6] Klinikum Gütersloh gGmbH, Gütersloh, Germany

Introduction

Pulmonary arterial hypertension (PAH) represents a progressive disease with currently insufficient treatment options, ultimately leading to right heart failure and death. Preclinical pharmacological treatment options have evolved in recent years aiming to target molecular pathways involved in the disease process. Numerous molecular abnormalities in different organs have been described in the pathogenesis of PAH (reviewed in (Paulin and Michelakis 2014)), but the prognosis

of PAH is still unfavorable. Current treatment strategies focus on vasodilation of the pulmonary vasculature and mainly target at lessening symptoms and improving quality of life.

PAH is characterized by elevated pulmonary vascular resistance (PVR) due to pulmonary vasoconstriction, pulmonary vascular remodelling, and thrombosis in situ. The underlying pathobiology of PAH is multifactorial (Rabinovitch 2008; Michelakis 2014; Rabinovitch et al. 2014). All layers of the vessel wall are involved in the process of pulmonary vascular remodelling. Thus, the composite of different cell types of the pulmonary arterial wall (endothelial cells, smooth muscle cells, and fibroblasts), as well as platelets and inflammatory cells, both in the vasculature and in the lung, may play a significant role in PAH (Yuan and Rubin 2005; Michelakis 2014), which, in turn, also represent potential therapeutic cellular targets.

There are several lines of evidence that patients with PAH have reduced expression of apolipoprotein E (ApoE) and peroxisome proliferator-activated receptor-γ (PPARγ) in lung tissue (Geraci et al. 2001; Ameshima et al. 2003). PPARγ agonistic treatment has primarily been shown to effectively ameliorate symptoms and signs of insulin resistance (Caglayan et al. 2005; Zaitone et al. 2015). PPARγ is a ligand-activated-transcription factor of the nuclear receptor superfamily, and PPARγ might also exert beneficial impact on pathways critically involved in the pathogenesis of PAH or on relaxation of pulmonary arteries (Nisbet et al. 2010; Kozlowska et al. 2013). In fact, studies demonstrated that insulin-resistant ApoE-deficient mice developed PAH that could be reversed by a PPARγ agonist (Hansmann et al. 2007). These data demonstrated that ApoE may be a risk factor for human PAH and that PPARγ activation can reverse PAH in animal models exhibiting metabolic disturbances.

Excessive pulmonary vascular remodelling is, in part, driven by medial and intimal hypertrophy based on proliferation of pulmonary arterial smooth muscle cells (PASMCs), which further are characterized by reduced susceptibility to apoptosis (Yuan and Rubin 2005). While current strategies to treat PAH aim at pulmonary vasodilation, recent efforts have been undertaken also targeting pulmonary vascular remodelling (Schermuly et al. 2005).

In addition, PAH is a driving force for progressive remodelling of the right ventricle (RV) due to high pressure afterload, which might result, eventually, in cardiomyocyte enlargement, alteration in phosphorylation patterns of contractile proteins, cardiac fibrosis, and ventricular decompensation associated with poor prognosis (Michelakis et al. 2008; Walker et al. 2011; Michelakis 2014).

Finally, several lines of evidence suggest inflammatory cells being activated in PAH, which facilitate or cause molecular changes through paracrine signalling. It was shown that PAH is, e.g., characterized by increased production of proinflammatory cytokines and perivascular inflammatory features (Lai et al. 2014; Paulin and Michelakis 2014). This also suggests that anti-inflammatory approaches might be promising to target PAH.

While most experimental studies have focused on prevention of PAH development (Matsuda et al. 2005; Kim et al. 2010; Dickinson et al. 2014), here we sought to elucidate the therapeutic impact of the PPARγ agonist pioglitazone in animals with established PAH. For this purpose, a model of induced PAH by monocrotaline in Sprague-Dawley rats was used to monitor the effect of pioglitazone on hemodynamics in the pulmonary circulation, cardiac and pulmonary vascular remodelling, and lung inflammation. The greater aims were (i) demonstration of insulin-sensitizing PPARγ as a molecular target for treatment of PAH, and (ii) dissecting the mechanisms of the beneficial effects of PPARγ treatment at different cellular- and tissue components of PAH.

Materials and methods

Animals

Adult male Sprague-Dawley rats (250 to 300 g) were purchased from Charles River (Charles River, Germany) and maintained in a temperature-controlled room with a 12:12 light-dark cycle. All animal care and experiments were performed in accordance with the German Laws for Animal Protections and were approved by the local animal care committee.

To induce PAH, monocrotaline (MCT, Sigma-Aldrich, Taufkirchen, Germany) was subcutaneously injected (60 mg/kg body weight, dissolved in 1 N HCl, and titrated to pH 7.4 with 1 N NaOH). Control animals were injected with the same volume of isotonic saline solution.

Twenty-one days after MCT-injection, a subset of rats was randomized either to regular chow or switched to pioglitazone treatment. Pioglitazone was administered via food pellets (40 mg/kg chow diet; Ssniff, Soest, Germany) for a period of 14 days. The mean daily drug dose of 2.5 mg/kg body weight was based on recommendations of Takeda. Pioglitazone was generously provided by Takeda (Takeda Pharmaceutical Company Limited, Kanagawa, Japan).

Rats were subjected to hemodynamic measurements at day 35 and were sacrificed thereafter. Organs were isolated and processed for immunohistochemical, histochemical/morphometric, and gene expression analyses.

Measurement of the pulmonary artery systolic pressure

At day 35 after MCT-injection, all rats were anesthetized with a pre-mixed combination of 100 mg/kg ketamine and 4 mg/kg xylazine, tracheostomized, and artificially ventilated. Right ventricular systolic pressure (RVSP), as a measure for PASP,

was determined utilizing a fluid-filled pressure catheter, inserted into the RV via the jugular vein. Systemic arterial pressure (SAP) was monitored in the carotid artery utilizing a 2 F Millar® microtip pressure catheter (Mil-SPR-302). The catheter information was amplified by a PowerLab® amplifier and converted to pressure curves using LabChart7® software (AD Instruments, Sydney, Australia). Three to five tracings from different time points were taken to determine the individual PASP and SAP.

Assessment of right ventricular hypertrophy

Subsequent to hemodynamic measurements, the heart was isolated, the RV was dissected from the LV and ventricular septum (S), and wet weights were obtained separately. RV hypertrophy was assessed by the ratio of the weight of RV to the weight of the LV free wall plus S [RV/(LV + S)] (Fulton's index) (Mam et al. 2010).

Evaluation of ventricular fibrosis

Cardiomyocyte cross-sectional area and interstitial fractional collagen content were determined in the RV and LV as measures of cardiac ventricle tissue remodelling. Three micrometer sections of the RV and LV were stained with hematoxylin and eosin and Massons' trichrome. Circumferences of 50 cardiomyocytes in each ventricle per animal were measured on transversely cut myocardial fibers. Microscopic images were analyzed in a blinded manner using Cell D Imaging Software. Transverse sections of the ventricles were taken to measure collagen content using Keyence software (Keyence, Germany). The percentage of collagen area was calculated on the entire slide for each rat.

Lung tissue preparation and morphometric analysis

Lungs were tracheally perfused with cold PBS and subsequently with 1 % paraformaldehyde, extracted and fixed in 4 % paraformaldehyde. Following dehydration, lungs were embedded in paraffin. Tissue blocks were sectioned for standard histological stainings (hematoxylin and eosin) and immunohistochemistry. Staining for α-actin (Sigma-Aldrich, USA), applying standard immunohistochemical protocols, was performed to quantify the degree of muscularization of pulmonary arteries. Morphometric analyses were performed using the Cell D Imaging Software (Olympus Soft Imaging Solution, Germany). The degree of muscularization was quantified by detection of α-actin positive parts of the vessel wall, which was defined as follows: non-muscularized: <5 %, partially muscularized 5–5 %, fully muscularized >75 %. The medial thickness was assessed in vessels (diameter <100 μm) indexed to terminal bronchioles. Lumen area was defined as the area within the lamina elastica interna, averaged from the same representative vessels. Distorted arteries were not used for the measurement. The percentage of medial wall thickness was calculated by the formula: medial wall thickness [%]: (2 × media thickness/external diameter) × 100.

Assessment of vascular proliferation and macrophage infiltration

For analyses of vascular proliferation indices, paraffin-embedded lung tissue sections were incubated with a mouse monoclonal antibody (mAb) against proliferating cell nuclear antigen (PCNA, 1:60, Dako, PC10) and biotinylated rabbit anti-mouse IgG (1:500, Dako) as a secondary antibody. Positive cells were stained using the Vectastain ABC Kit PK-6100 and the peroxidase substrate kit DAB SK-4100 (both Vector). The tissues were counterstained with hematoxylin. Pictures were acquired at ×40 magnification at room temperature and cells were counted. Analyses are expressed as PCNA-positive cells per total cell number of each artery. For analyses of macrophage lung infiltration, the rat macrophage marker ED-2 (anti-CD 68, AbD Serotec, Germany) was used, followed by standard immunohistochemical protocols. For each animal, absolute numbers of macrophages/mm^2 were counted in ten randomly chosen fields at ×200 magnification using Cell D Imaging Software.

Gene expression profiling

For quantitative real-time RT-PCR (qPCR), the lung, RV, and LV were excised from all animal groups and shock-frozen, followed by lysis in RLT buffer (Qiagen) and RNA extraction applying the RNeasy Mini Kit (Qiagen). The High Capacity RNA-to-cDNA Kit (Applied Biosystems) was used for cDNA synthesis. Gene expression analysis by qPCR (SybrGreen®) was done in duplicate or triplicate with an Mx3000P cycler (Stratagene; Agilent Technologies, La Jolla, CA) and normalized to HPRT. Primer sequences (all used at final concentration of 100 nM) were as follows (forward primer, reverse primer, respectively):

hypoxanthine-guanine-phophoribosyl-transferase (HPRT): CTCATGGACTGATTATGGACA-GGAC, GCAGGTCAGCAAAGAACTTATAGCC; brain natriuretic peptide (BNP): GAAGATAGACCGGATCGGCG, TCCCAGAGCTGGGGAAAGAA; and osteopontin: CCAGCCA-AGGACCAACTACA, TGGCTACAGCATCTGAGTGTT.

Statistical analysis

Data are expressed as means ± SEM. For gene expression analyses, group comparison was done by Dunn's test. All other data were analyzed by one-way ANOVA followed by post hoc Student-Newman-Keuls (SNK) tests. Kaplan-Meier statistics were used for survival analysis. The log-rank

(Mantel-Cox) test was used to compare survival curves. A P value of <0.05 was regarded as significant.

Results

Effects of MCT and PPARγ activation on systemic blood pressure, pulmonary hemodynamics, and survival

Rats were subjected either to a control group with saline injection or a PAH-induction group with MCT-injection. The PAH-induction group was further divided into a group receiving a control or a pioglitazone-enriched chow starting 21 days after PAH-induction for additional 2 weeks.

Figure 1a depicts the Kaplan-Meier curve, demonstrating that all control rats survived until day 35. Rats subjected to MCT-injection developed not only severe PAH (below) but were also characterized by a reduced survival during the 35 days of follow-up. While in the MCT-group, survival was reduced by 55 %, in the pioglitazone group, survival rates were reduced by 24 % within the experimental period. In addition, no animal died within the 35 days follow-up in an additional control group with pioglitazone without MCT-injection ($N=3$, not shown).

At day 35, SAP [mmHg] and the PASP [mmHg] were measured. While SAP was neither significantly altered by MCT, nor by additional treatment with pioglitazone (Fig. 1b), MCT-injection led to PAH characterized by a significant increase of PASP from 28.6 ± 2.3 mmHg to 74.9 ± 4.1 mmHg (Fig. 1c). The treatment approach with pioglitazone significantly reduced PASP to 61.4 ± 4.5 mmHg, while pioglitazone in a healthy control group without MCT-injection did not change the PASP compared to the control group (32.9 ± 1.3 mmHg, $N=3$, not shown).

Taken together, MCT resulted in enhanced PASP accompanied with reduced survival, which was partially reverted by pioglitazone.

Structural analyses of right ventricular hypertrophy and muscularization rates

MCT-injection resulted in major pulmonary vascular remodelling indicated by a significantly increased medial wall thickness. Figure 2a depicts representative specimens subjected to hematoxylin-eosin or α-actin staining of the pulmonary tissues derived from rats subjected to control treatment, MCT, or MCT and pioglitazone. MCT-injection was followed by a marked increase in vascular remodelling, evidenced by enhanced α-actin (Fig. 2a, middle), which was clearly reduced in animals that were subjected to additional pioglitazone treatment (Fig. 2a, right).

Muscularization of pulmonary arteries critically impacts hemodynamics. We thus quantified the proportion of non- (N), partially (P), or fully (M) muscularized pulmonary arteries, as percentage of total pulmonary artery cross section in intraacinar vessels sized <100 μm of each rat (Fig. 2b). While MCT was demonstrated to enhance muscularization, partial reversal was seen by additional pioglitazone treatment (Fig. 2b). MCT-injection resulted in 56.6 ± 10.1 % fully muscularized arteries, compared to 5.0 ± 2.4 % in the control group. This increase in muscularization was accompanied by virtual loss of non-muscularized arteries, whereas in the control group 72.4 ± 6.3 % were non-muscularized. Pioglitazone treatment reduced the amount of muscularized arteries. Fully muscularized arteries were detected by 19.9 ± 8.0 %, and partially muscularized arteries were seen in 77.3 ± 8.5 %, respectively, whereas non-muscularized arteries were 2.8 ± 1.6 % in rats subjected to pioglitazone.

Besides muscularization proportions, medial wall thickness and lumen area of pulmonary arteries were quantified. Medial wall thickness was markedly increased in arteries sized <100 μm in diameter from 10.2 ± 1.7 % (control) to 26.1 ± 1.7 % in the MCT group (Fig. 2c). In the pioglitazone group, the increase of medial wall thickness was significantly reversed to 20.5 ± 1.1 %, demonstrating the anti-remodelling impact of pioglitazone on the pulmonary vasculature (Fig. 2c). Finally, lumen area of pulmonary arteries (measured in μm^2) was significantly decreased in the MCT group from 1985.3 ± 506.8 μm^2 to 1005.0 ± 86.6 μm^2 ($P<0.05$) and treatment with pioglitazone resulted in an increase by 466.3 μm^2 (n.s. compared to the MCT group) (Fig. 2d).

Since MCT-injection resulted in vascular remodelling, characterized by reduced lumen and enhanced medial wall thickness, we next explored the proliferation rates within pulmonary arteries. As shown in Fig. 3a, b, cell proliferation—measured by immunohistochemical stainings against proliferating cell nuclear antigen (PCNA)—was significantly higher in the MCT group (24.5 ± 3.8 % positive cells) compared to the control group (8.2 ± 2.4 %) ($P<0.01$). The MCT-induced increase was effectively reduced by pioglitazone treatment (11.6 ± 1.9 %; $P<0.01$ compared to MCT).

Thus, pulmonary hypertension, induced by MCT, is characterized by vascular remodelling associated with enhanced proliferation, which is significantly reduced in rats subjected to pioglitazone.

Right and left ventricular remodelling

One major obstacle in pulmonary hypertension is the consecutive impact on structural RV and LV remodelling and/or fibrosis. Figure 4a depicts representative hematoxylin-eosin stainings of all three animal groups. We measured the cross-sectional area (CSA) of cardiomyocytes as one parameter of ventricular remodelling. MCT lead to significantly enhanced CSA in the RV from 187.9 ± 11.6 μm^2 to 448.2 ± 48.1 μm^2 (control group and MCT group, respectively, $P<0.001$)

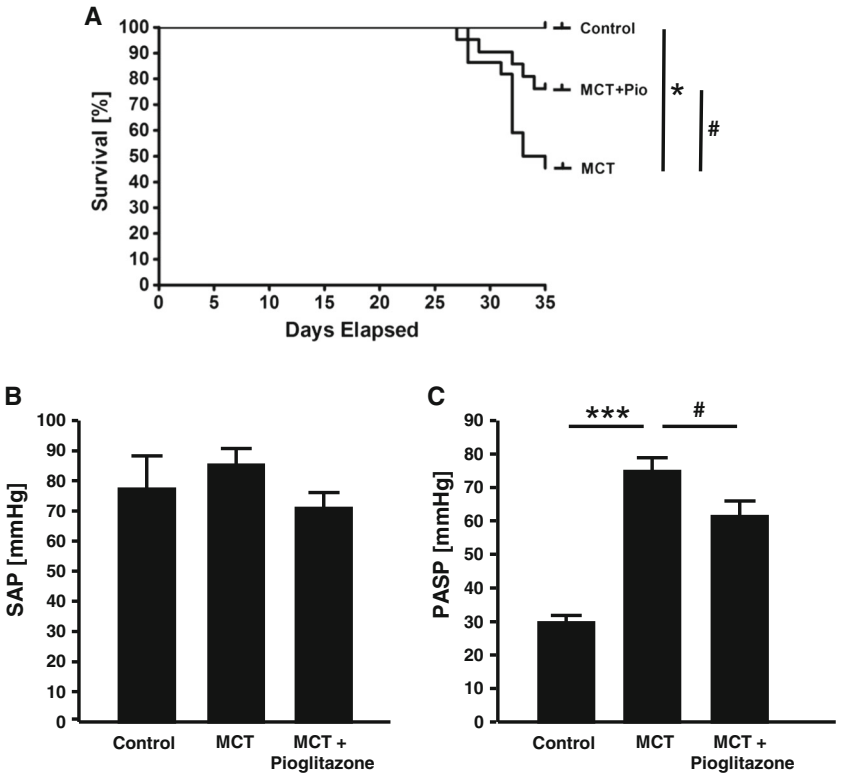

Fig. 1 Impact of pioglitazone on survival rates and hemodynamics in MCT-induced pulmonary hypertension. **a** MCT or saline was injected at day 0, pioglitazone treatment (2.5 mg/kg body weight) started 21 days thereafter for the following 14 days. Survival rates of control, MCT-treated, and MCT + pioglitazone-treated animals are shown (*$P < 0.05$ control vs MCT; $^{\#}P < 0.05$ MCT vs MCT + Pio) (control $N = 9$; MCT + Pio $N = 22$; MCT + pioglitazone $N = 21$). **b** Systemic arterial pressure (SAP; in mmHg) (control $N = 5$; MCT $N = 6$; MCT + pioglitazone $N = 7$). **c** Pulmonary artery systolic pressure (PASP) were determined as stated in the "Materials and Methods" section (***$P < 0.001$ control vs MCT; $^{\#}P < 0.05$ MCT vs MCT + pioglitazone) (control $N = 6$; MCT $N = 6$; MCT + pioglitazone $N = 9$)

(Fig. 4b), while the CSA remained largely unchanged in LV (Fig. 4c). Pioglitazone was capable to reduce the CSA increase in the RV (235.4 ± 18.0 μm^2; $P < 0.001$ compared to MCT) (Fig. 4b).

Quantitative PCR was applied to analyze differential gene expression in animal groups in whole lung tissue. BNP is an established target gene in heart failure and ventricular remodelling. BNP was significantly enhanced on transcript levels (15.6 ± 1.5-fold of control, $P < 0.001$), and pioglitazone reduced ventricular BNP gene expression (11.4 ± 1.0-fold of control) (Fig. 4d).

The RV hypertrophy was further evaluated by postmortem measurement of the weight of the RV, the LV, and the septum (S) and is expressed as a ratio (RV/LV + S) (Fulton's index). Fulton's index was 0.26 ± 0.05 in control animals. It was enhanced to 0.56 ± 0.02 with MCT and significantly reduced to 0.52 ± 0.02 with pioglitazone treatment (Fig. 4e). The absolute RV weight also increased from 236.4 ± 34.9 mg to 454.2 ± 14.9 mg with MCT and was reduced to 419.6 ± 16.7 mg with MCT + pioglitazone (not shown, LV + S 898.8 ± 31.8 mg (control); 795.6 ± 24.9 (MCT), and 807.2 ± 25.5 (MCT + pioglitazone), respectively). However, similar to the functional impact of PPARγ activation on MCT-induced PAH (Fig. 1c), RV hypertrophy was only moderately reversed by pioglitazone treatment (Fig. 4e).

Right and left ventricular fibrosis

After we established a significant impact of MCT on cardiomyocyte size and RV hypertrophy, with pioglitazone partially capable to revert these changes, we next aimed at evaluating fibrotic remodelling in both RV and LV. As shown in Fig. 5a–c, fibrosis, measured by Massons' trichrome histological staining, was significantly enhanced from 1.2 ± 0.2 to 29.8 ± 5.4 % in rats subjected to MCT-induced PAH, and pioglitazone was clearly effective in reducing the area of fibrotic tissue in the RV to 10.8 ± 1.0 % (Fig. 5b). Interestingly, in contrast to unaltered CSA (Fig. 4c), fibrosis was also enhanced in the LV from 0.4 ± 0.4 to 21.4 ± 3.4 % with MCT, with pioglitazone capable in reducing the amount of fibrosis rate (8.6 ± 1.7 %) as well (Fig. 5c).

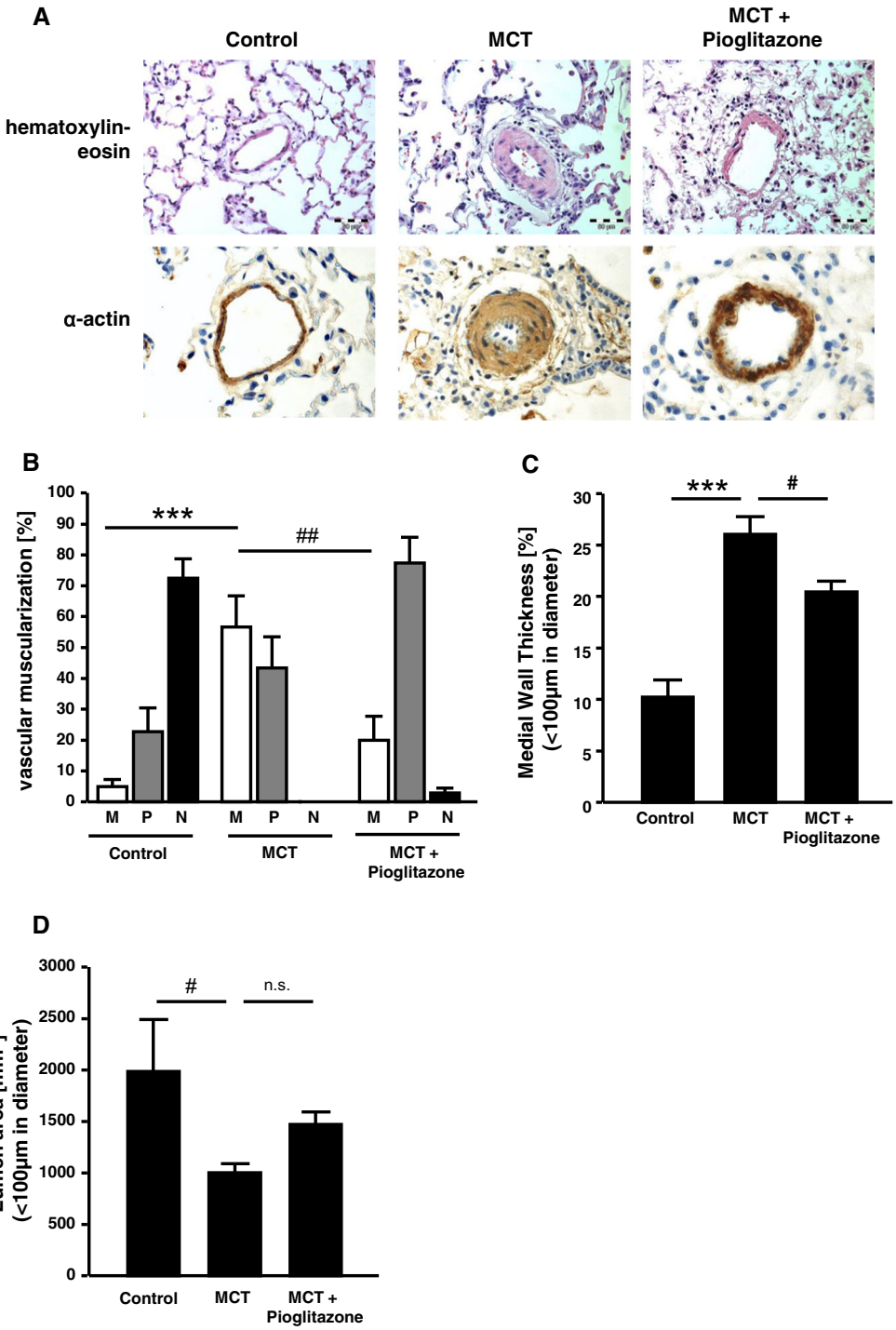

Fig. 2 Effect of pioglitazone on pulmonary vascular remodelling in MCT-induced pulmonary hypertension. **a** Shown are representative hematoxylin-eosin and immunohistochemical stainings (against α-actin, as a measure of the degree of muscularization) in rats subjected to control treatment (*left*), MCT-injection (*middle*), or MCT and additional pioglitazone treatment (*right*). Scale bars 100 μm. **b** Quantification of vascular muscularization was done in the lung arteries sized <100 μm. Shown are the proportions of non- (N), partially (P), or fully (M) muscularized pulmonary arteries as the percentage of total pulmonary artery cross section. A total of 11–14 intraacinar vessels per section were analyzed in each rat lung. In total, $N = 16$ animals were analyzed. (***$P < 0.001$ control vs MCT; $^{\#\#}P < 0.05$ MCT vs MCT + Pioglitazone) (control $n = 42/N = 3$; MCT $n = 66/N = 6$; MCT + Pioglitazone $n = 91/N = 7$ arteries). **c** Quantification of medial wall thickness of pulmonary arteries sized <100 μm in diameter is shown (***$P < 0.001$ control vs MCT; $^{\#}P < 0.05$ MCT vs MCT + Pioglitazone) (control $n = 42/N = 3$; MCT $n = 66/N = 6$; MCT + Pioglitazone $n = 91/N = 7$ arteries). **d** The internal lumen areas of vessels <100 μm in diameter are shown ($^{\#}P < 0.05$ control vs MCT; *n.s.* non-significant)

Pulmonary macrophage content

Besides pulmonary vascular remodelling, cardiac hypertrophy and fibrosis, inflammatory signals, and macrophage invasion have been shown to represent key features in pulmonary hypertension. We thus evaluated the macrophage content in the lungs of all three animal groups (Fig. 6a, b). The amount of macrophages, determined as cells/mm^2, in the lungs of MCT-treated rats was significantly higher than in the control group (84.1 ± 8.3 cells/mm^2 vs 4.2 ± 0.2 cells/mm^2, respectively, $P < 0.001$) (Fig. 6a, b). While pioglitazone treatment was followed by >40 % reduction in macrophages, the amount of macrophages, however, remained higher than in the control group (47.3 ± 4.9 cells/mm^2) ($P < 0.01$ compared to MCT).

One trigger of monocyte evasion and macrophage transformation in the lung tissue in pulmonary hypertension might be

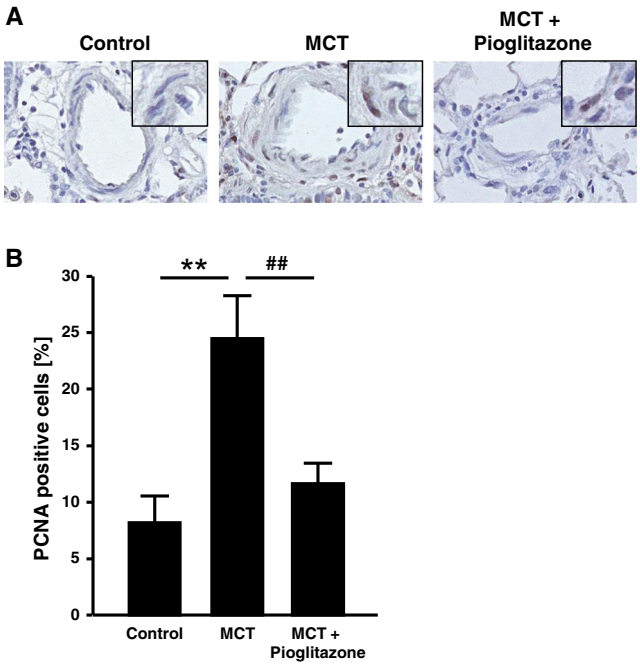

Fig. 3 Effect of pioglitazone on pulmonary smooth muscle cell proliferation. **a** Shown are representative immunohistochemical stainings of the lung tissues against proliferating cell nuclear antigen (PCNA) of control-, MCT-, and MCT + Pioglitazone-treated animals with insets for better visualization of positive cells. **b** Quantification of PCNA-positive cells is shown (**$P < 0.01$ Control vs MCT; $^{\#\#}P < 0.01$ MCT vs MCT + Pioglitazone) (control $N = 8$; MCT $N = 9$; MCT + Pioglitazone $N = 9$)

enhanced content of osteopontin. Osteopontin is not only an extracellular matrix protein, but also a chemoattractant for monocytes in inflammatory tissue remodelling. When measuring transcript levels in total lung tissue, osteopontin gene expression was significantly higher in the MCT group (75.1 ± 9.6-fold of control, $P < 0.001$), and pioglitazone treatment effectively reduced osteopontin levels (50.5 ± 6.8-fold of control, $P = 0.067$ compared to MCT) (Fig. 6c).

Thus, besides beneficial hemodynamical and structural changes in the lung and heart by pioglitazone, also inflammatory signals were effectively reduced.

Discussion

In this study we demonstrate that in a model of MCT-induced PAH development in adult male Sprague-Dawley rats, PPARγ activation by pioglitazone was effective in reducing RV pressure, pulmonary artery remodelling, and proliferation. Further, pioglitazone partially reverted MCT-induced upregulation of BNP in the RV, as well as myocyte enlargement and cardiac fibrotic remodelling. Besides anti-remodelling effects of PPARγ activation, pioglitazone was also capable in effectively reducing PAH-associated lung inflammation, characterized by reduction of macrophage content and osteopontin gene expression. Finally, survival was significantly improved by pioglitazone within the experimental time frame. Taken together, activation of PPARγ with pioglitazone represents a valid target to ameliorate MCT-induced PAH. To our knowledge, this is the first report analyzing the effect of the PPARγ activator pioglitazone in an established model of MCT-induced pulmonary hypertension.

PAH represents a disease with limited therapeutic options and a current life expectancy comparable to metastatic cancers (Michelakis 2014). Clinical approaches are based on vasodilation by endothelin receptor blockade, PDE5 inhibition, sGC stimulation and activation of the prostacyclin pathway, as well as symptomatic treatment. Later advances, both experimentally and clinically, were based on targeting pulmonary vascular remodelling by inhibiting the PDGF beta-receptor (Schermuly et al. 2005) to mainly reduce vascular smooth muscle cell proliferation. However, PAH-associated remodelling is believed to involve both vascular and heart remodelling processes and inflammatory changes in the lung (Ryan et al. 2015). PPARγ functions as a transcriptional regulator, particularly in adipose tissue where it regulates mainly genes involved in glucose and lipid metabolism (Lee et al. 2003). Even though PPARγ is abundantly expressed in adipose tissue, significant expression has also been detected in cells within the vessel wall (monocytes/macrophages, endothelial cells, and vascular smooth muscle cells) (Hsueh et al. 2001). Identified as a therapeutic target, PPARγ agonists have initially been clinically introduced as insulin-sensitizing treatment. In experimental models, ApoE-deficiency was earlier been proven leading to development of PAH with the PPARγ agonist rosiglitazone reducing PAH-associated vascular remodelling (Hansmann et al. 2007). These data demonstrated that ApoE may be a risk factor for PAH and that PPARγ activation can reverse PAH in an animal model exhibiting metabolic disturbances. In addition, rosiglitazone was effective in pulmonary hypertension models that were based on hypoxia-induced PAH (Crossno et al. 2007; Nisbet et al. 2010). Here, we applied an MCT-based model of PAH in rats for dissecting the impact of pioglitazone on vascular proliferation and remodelling, RV and LV hypertrophy and fibrosis, PASP, and lung inflammation. The MCT model is particularly informative in the context of inflammation. In addition, pulmonary vasoconstriction seems to be an important mechanistic component. MCT is believed to cause direct endothelial cell injury with subsequent accumulation of inflammatory mononuclear cells in the vascular wall, which finally induces proliferation and migration of vascular smooth muscle cells. In addition, a profound remodelling of the heart with RV hypertrophy and dysfunction occurs in contrast to other experimental models of PAH (Stenmark et al. 2009). We have particularly chosen this model, since we hypothesized from our previous studies that pioglitazone attenuates vascular and myocardial remodelling, as well as inflammation, features which all are believed to contribute to PAH.

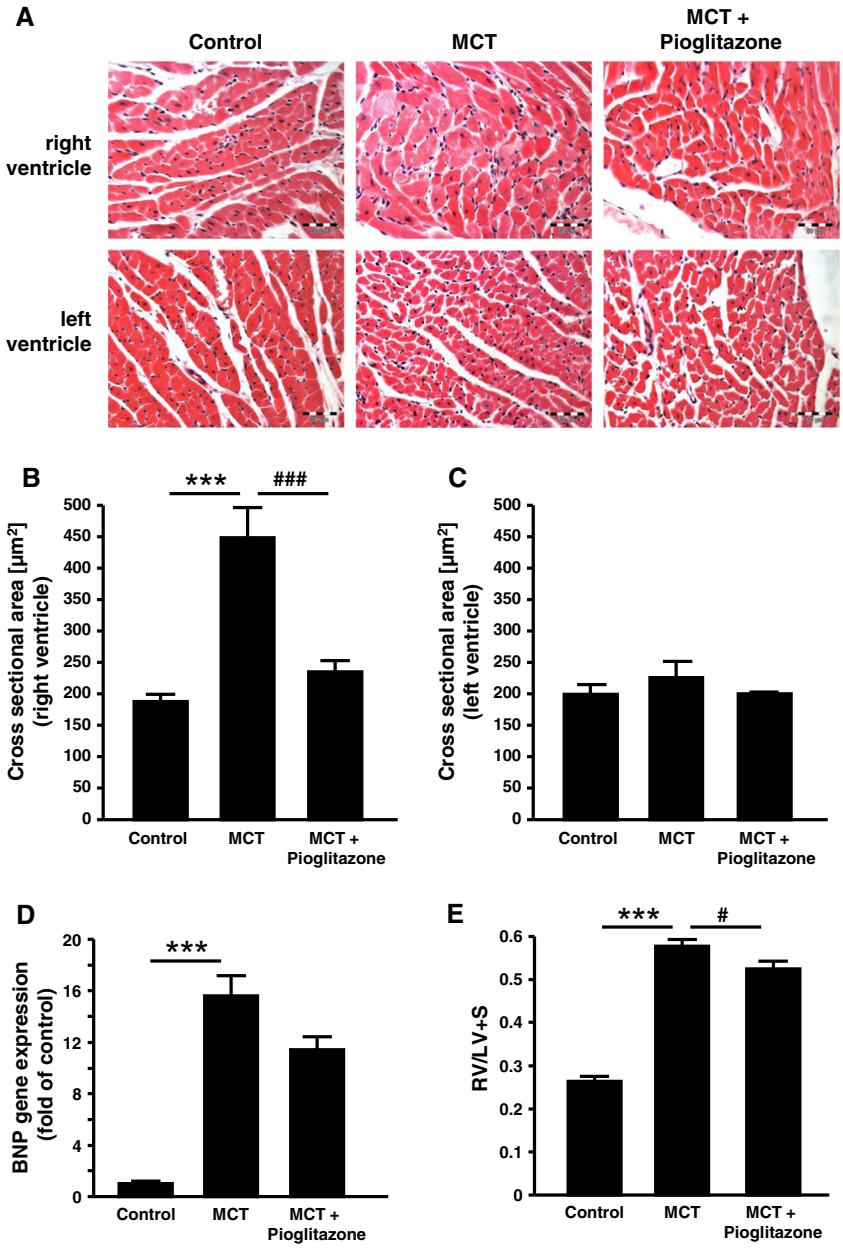

Fig. 4 Impact of pioglitazone on the right and left ventricle remodelling and hypertrophy in MCT-induced pulmonary hypertension. **a** Representative hematoxylin-eosin stainings of the right ventricle (*upper panel*) and the left ventricle (*lower panel*) derived from control-, MCT-, and MCT + Pioglitazone-treated animals. Scale bars 100 µm. **b** Myocyte cross section area (in μm^2) in the right ventricle in each study group (***$P < 0.001$ control vs MCT; ###$P < 0.001$ MCT vs MCT + Pioglitazone) (50 cells per animal for 5 animals per group). **c** Myocyte cross section area (in μm^2) in the left ventricle in each study group (control $N = 5$; MCT $N = 5$; MCT + Pioglitazone $N = 5$). **d** Relative gene expression of brain natriuretic peptide (BNP) in the right ventricle in each study group. Transcript levels were determined by quantitative real-time PCR analysis, and were normalized to the expression of *HPRT*. The expression of control rats was arbitrarily set as 1 (***$P < 0.001$ control vs MCT) (control $N = 6$; MCT $N = 11$; MCT + Pioglitazone $N = 11$). **e** Right ventricle (RV) to left ventricle (LV) + septum (S) ratios of rats from each study group are shown (***$P < 0.001$ control vs MCT; #$P < 0.05$ MCT vs MCT + Pioglitazone) (control $N = 9$; MCT $N = 21$; MCT + Pioglitazone $N = 19$)

MCT-induced PAH is an aggressive model with rapid progression towards death, with the animals suffering from severe sickness. Survival in the MCT group was reduced by 55 % at day 35 after MCT-injection. In this manuscript, we aimed to model a disease state of established PAH with manifest end organ damage. Established PAH is usually the clinical scenario where a pharmacologic treatment is started in PAH patients. Therefore, we were interested in testing pioglitazone under these circumstances.

The novel finding in the present study is that pioglitazone is effectively ameliorating PASP, along with heart remodelling and lung inflammation and improved survival, in an MCT-based model without metabolic disorders. Moreover, in our study pioglitazone is capable in addressing multiple molecular abnormalities simultaneously, indicating a potential superordinate role interfering in the complex disease process of PAH.

We have analyzed the impact of pioglitazone on different outcomes of pulmonary hypertension. It has to be stressed that PASP was significantly lowered by pioglitazone treatment; however, the MCT-induced increase was not fully abrogated. Nonetheless, we cannot rule out that higher doses of pioglitazone than used in our study (2.5 mg/kg body weight) would have been even more effective. A recent study applying pioglitazone in a flow-induced PAH-model also demonstrated lowering but not blunting of increased PASP, which is in accordance with our data, even at doses of 20 mg/kg body weight (Dickinson et al. 2014). Thus, it is more likely that

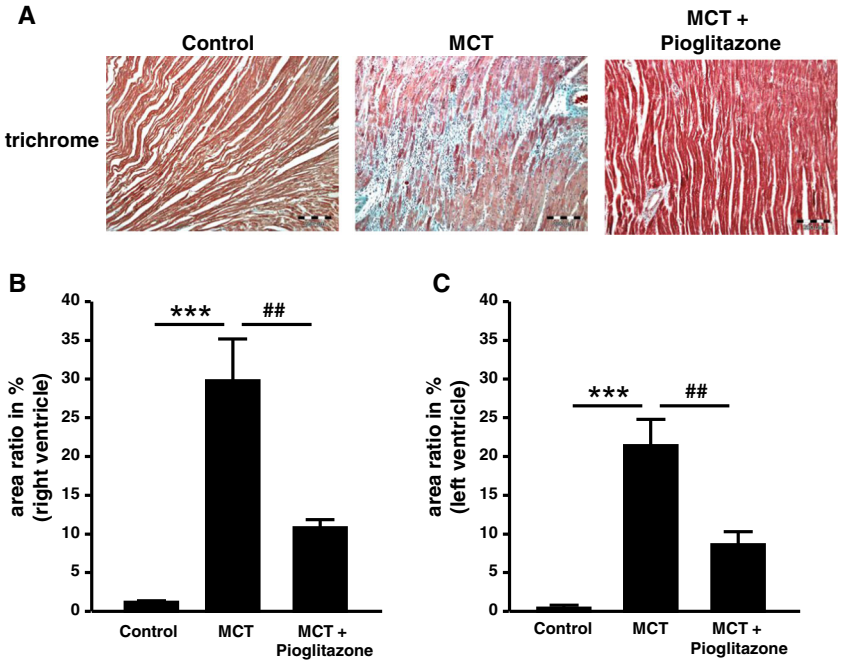

Fig. 5 Effect of pioglitazone on fibrosis in MCT-induced pulmonary hypertension. **a** Interstitial collagen content applying histological Massons' trichrome stainings. Shown are representative photomicrographs from each study group. Scale bars 100 μm. **b** Quantification of collagen content in the right ventricle measured as the collagen-positive area in percent (***$P < 0.001$ Control vs MCT; $^{\#\#}P < 0.01$ MCT vs MCT + Pioglitazone) (Control $N = 5$; MCT $N = 5$; MCT + Pioglitazone $N = 5$). **c** Quantification of collagen content in the left ventricle as in (**b**) (***$P < 0.001$ Control vs MCT; $^{\#\#}P < 0.01$ MCT vs MCT + Pioglitazone) (Control $N = 5$; MCT $N = 5$; MCT + Pioglitazone $N = 5$)

other pathways in addition to PPARγ signalling play a general role in PAH-associated remodelling.

BNP represents the clinically most valuable biomarker of chronic pressure overload and ventricular volume. In patients with PAH, BNP has been demonstrated to correlate with PASP (Palazzuoli et al. 2015; ten Freyhaus et al. 2015). In line with others, BNP gene expression was upregulated in MCT-induced PAH in the RV (Dias-Neto et al. 2015), confirming cardiac overload. This was effectively reversed by pioglitazone treatment. BNP expression has earlier been shown to

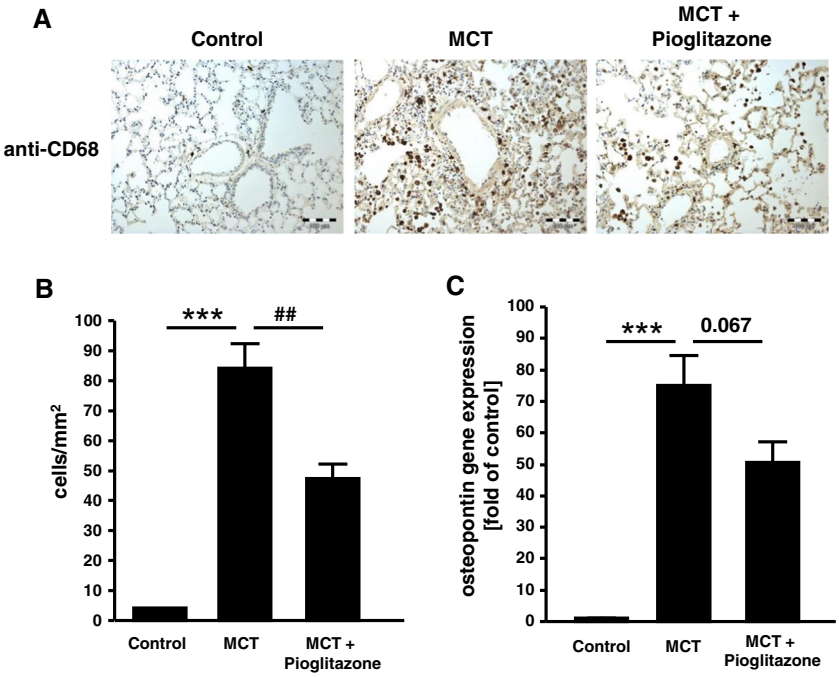

Fig. 6 Impact of pioglitazone on lung inflammation in MCT-induced pulmonary hypertension. **a** Shown are representative lung immunohistochemical stainings with antibodies against CD68 for detection of macrophages in each study group. Scale bars 100 μm. **b** Quantification of CD68-positive cells (***$P < 0.001$ Control vs MCT; $^{\#\#}P < 0.01$ MCT vs MCT + Pioglitazone) (ten high power fields per animal and three to five animals per group). **c** Relative gene expression of osteopontin total lung tissues derived from animals of each study group. Transcript levels were determined by quantitative real-time PCR analysis, and were normalized to the expression of *HPRT*. The expression of control rats was arbitrarily set as 1 (***$P < 0.001$ Control vs MCT) (control $N = 7$; MCT $N = 10$; MCT + Pioglitazone $N = 16$)

be increased after 21 days, but not as early as 1 or 7 days after MCT-application (Dias-Neto et al. 2015). Here, we applied pioglitazone in a treatment but not preventive approach, since it was given 21 days after MCT-injection for a 14 day period. Thus, in accordance with reduced PASP, pioglitazone lowered RV overload which is reflected by downregulation of BNP gene expression. Further, the MCT-induced increase in cardiomyocyte hypertrophy, which was accompanied by enhanced fibrosis, was significantly reduced by pioglitazone treatment. While the diameter of cardiomyocytes was only enhanced in the RV, higher fibrosis in PAH animals was detected in both RV and LV. The increase in fibrosis but absence in enhanced cardiomyocyte diameter in the LV suggests that other factors are responsible for these fibrotic remodelling processes. Nonetheless, pioglitazone effectively decreased fibrosis in both ventricles, substantiating the beneficial impact of PPARγ activation on multiple pathophysiological entities relevant in PAH. The significant effect of pioglitazone on, e.g., RV remodelling is also reflected by lowered Fulton's index. Again, in line with others, the ratio of RV/[LV + septum] was lowered (Dickinson et al. 2014), but not fully reversed by pioglitazone pointing towards partially irreversible cardiac remodelling processes induced by MCT.

On a vascular level, MCT increased medial thickening in small pulmonary arteries, as expected (Michelakis et al. 2008). This increase was accompanied by both reduced lumen area and enhanced vascular muscularization. These remodelling processes, ultimately increasing vascular resistance, are particularly triggered by proliferation and migration of pulmonary arterial smooth muscle cells (PASMCs). Indeed, enhanced proliferation of PASMCs within the vascular wall were detected in MCT-induced PAH in small arteries sized <100 μm, which was evidenced by PCNA staining. PPARγ agonists have earlier been shown to reduce proliferation of PASMCs (Li et al. 2010). Conversely, deletion of PPARγ in PASMCs causes vascular remodelling and increased muscularization in PAH (Hansmann et al. 2008). Others could show that rosiglitazone—given as a prevention approach—was capable in reducing PASMC proliferation in hypoxia-induced PAH models (Nisbet et al. 2010). Here, we demonstrate that pioglitazone is effective in downregulating PASMC proliferation in rats, even when administered at a time point, when neointimal hyperplasia in small pulmonary arteries had already occurred, stressing the impact of pioglitazone on already stimulated and ongoing vascular remodelling processes.

Finally, we evaluated the potential influence of pioglitazone on processes besides vascular and cardiac remodelling. Thus, analyzing pulmonary inflammation by determining abundance of macrophages in the lung, MCT-induced PAH was associated with highly elevated content of CD68-positive cells. Dissecting potential triggers for monocyte evasion and macrophage transformation, we measured osteopontin gene expression in the lung. Osteopontin represents a proinflammatory cytokine, exerting chemoattractant properties, which has been implicated in numerous tissue remodelling processes including diabetic nephropathy (Tachibana et al. 2012), cancer (Ota et al. 2014), LV hypertrophy (Hou et al. 2014), and fibrosis (Caglayan et al. 2008). Further, it was shown that PPARγ-responsive region lies between −1000 bp and −970 bp relative to the osteopontin promoter transcription start site (Oyama et al. 2002). In line with increased levels of macrophages in rats characterized by PAH, osteopontin gene expression in the lung was significantly increased. Strikingly, osteopontin transcripts were lowered associated with reduced macrophages in the lung tissue in the animal group receiving pioglitazone. This anti-inflammatory impact of pioglitazone is also in accordance with observations of reduced cardiac and adipose tissue inflammation in metabolic (Rangwala and Lazar 2004; Matsuura et al. 2015) and non-metabolic animal models (Gao et al. 2015).

To summarize, here, we show that the insulin-sensitizer pioglitazone is an effective drug-reducing multiple pathological entities in MCT-induced PAH, including RV remodelling, PASMC proliferation, pulmonary vascular thickening and muscularization, and lung inflammation, even in the absence of metabolic disturbances. Importantly, these beneficial effects were detectable when pioglitazone was administered as a therapeutic approach in an animal model with developed PAH, also ultimately leading to enhanced survival.

Acknowledgments This study was supported by the Marga und Walter Boll-Stiftung (210-04-10) to K.K. and E.C. M.T. is supported by a PhD scholarship of the Charité-Nachwuchskommission.

Compliance with ethical standards All animal care and experiments were performed in accordance with the German Laws for Animal Protections and were approved by the local animal care committee.

References

Ameshima S, Golpon H, Cool CD, Chan D, Vandivier RW, Gardai SJ, Wick M, Nemenoff RA, Geraci MW, Voelkel NF (2003) Peroxisome proliferator-activated receptor gamma (PPARgamma) expression is decreased in pulmonary hypertension and affects endothelial cell growth. Circ Res 92:1162–1169

Caglayan E, Blaschke F, Takata Y, Hsueh WA (2005) Metabolic syndrome-interdependence of the cardiovascular and metabolic pathways. Curr Opin Pharmacol 5:135–142

Caglayan E, Stauber B, Collins AR, Lyon CJ, Yin F, Liu J, Rosenkranz S, Erdmann E, Peterson LE, Ross RS, Tangirala RK, Hsueh WA (2008) Differential roles of cardiomyocyte and macrophage peroxisome proliferator-activated receptor gamma in cardiac fibrosis. Diabetes 57:2470–2479

Crossno JT Jr, Garat CV, Reusch JE, Morris KG, Dempsey EC, McMurtry IF, Stenmark KR, Klemm DJ (2007) Rosiglitazone attenuates hypoxia-induced pulmonary arterial remodeling. Am J Physiol Lung Cell Mol Physiol 292:L885–L897

Dias-Neto M, Luisa-Neves A, Pinho S, Goncalves N, Mendes M, Eloy C, Lopes JM, Goncalves D, Ferreira-Pinto M, Leite-Moreira AF, Henriques-Coelho T (2015) Pathophysiology of infantile pulmonary

arterial hypertension induced by monocrotaline. Pediatr Cardiol 36: 1000–1013

Dickinson MG, Kowalski PS, Bartelds B, Borgdorff MA, van der Feen D, Sietsma H, Molema G, Kamps JA, Berger RM (2014) A critical role for Egr-1 during vascular remodelling in pulmonary arterial hypertension. Cardiovasc Res 103:573–584

Gao M, Jiang Y, Xiao X, Peng Y, Yang M (2015) Protective effect of pioglitazone on sepsis-induced intestinal injury in a rodent model. J Surg Res 195:550–558

Geraci MW, Moore M, Gesell T, Yeager ME, Alger L, Golpon H, Gao B, Loyd JE, Tuder RM, Voelkel NF (2001) Gene expression patterns in the lungs of patients with primary pulmonary hypertension: a gene microarray analysis. Circ Res 88:555–562

Hansmann G, Wagner RA, Schellong S, Perez VA, Urashima T, Wang L, Sheikh AY, Suen RS, Stewart DJ, Rabinovitch M (2007) Pulmonary arterial hypertension is linked to insulin resistance and reversed by peroxisome proliferator-activated receptor-gamma activation. Circulation 115:1275–1284

Hansmann G, de Jesus Perez VA, Alastalo TP, Alvira CM, Guignabert C, Bekker JM, Schellong S, Urashima T, Wang L, Morrell NW, Rabinovitch M (2008) An antiproliferative BMP-2/PPARgamma/apoE axis in human and murine SMCs and its role in pulmonary hypertension. J Clin Invest 118:1846–1857

Hou X, Hu Z, Huang X, Chen Y, He X, Xu H, Wang N (2014) Serum osteopontin, but not OPN gene polymorphism, is associated with LVH in essential hypertensive patients. J Mol Med (Berl) 92:487–495

Hsueh WA, Jackson S, Law RE (2001) Control of vascular cell proliferation and migration by PPAR-gamma: a new approach to the macrovascular complications of diabetes. Diabetes Care 24:392–397

Kim EK, Lee JH, Oh YM, Lee YS, Lee SD (2010) Rosiglitazone attenuates hypoxia-induced pulmonary arterial hypertension in rats. Respirology 15:659–668

Kozlowska H, Baranowska-Kuczko M, Schlicker E, Kozlowski M, Kloza M, Malinowska B (2013) Relaxation of human pulmonary arteries by PPARgamma agonists. Naunyn Schmiedeberg's Arch Pharmacol 386:445–453

Lai YC, Potoka KC, Champion HC, Mora AL, Gladwin MT (2014) Pulmonary arterial hypertension: the clinical syndrome. Circ Res 115:115–130

Lee CH, Olson P, Evans RM (2003) Minireview: lipid metabolism, metabolic diseases, and peroxisome proliferator-activated receptors. Endocrinology 144:2201–2207

Li M, Li Z, Sun X, Yang L, Fang P, Liu Y, Li W, Xu J, Lu J, Xie M, Zhang D (2010) Heme oxygenase-1/p21WAF1 mediates peroxisome proliferator-activated receptor-gamma signaling inhibition of proliferation of rat pulmonary artery smooth muscle cells. FEBS J 277: 1543–1550

Mam V, Tanbe AF, Vitali SH, Arons E, Christou HA, Khalil RA (2010) Impaired vasoconstriction and nitric oxide-mediated relaxation in pulmonary arteries of hypoxia- and monocrotaline-induced pulmonary hypertensive rats. J Pharmacol Exp Ther 332:455–462

Matsuda Y, Hoshikawa Y, Ameshima S, Suzuki S, Okada Y, Tabata T, Sugawara T, Matsumura Y, Kondo T (2005) Effects of peroxisome proliferator-activated receptor gamma ligands on monocrotaline-induced pulmonary hypertension in rats. Nihon Kokyuki Gakkai Zasshi 43:283–288

Matsuura N, Asano C, Nagasawa K, Ito S, Sano Y, Minagawa Y, Yamada Y, Hattori T, Watanabe S, Murohara T, Nagata K (2015) Effects of pioglitazone on cardiac and adipose tissue pathology in rats with metabolic syndrome. Int J Cardiol 179:360–369

Michelakis ED (2014) Pulmonary arterial hypertension: yesterday, today, tomorrow. Circ Res 115:109–114

Michelakis ED, Wilkins MR, Rabinovitch M (2008) Emerging concepts and translational priorities in pulmonary arterial hypertension. Circulation 118:1486–1495

Nisbet RE, Bland JM, Kleinhenz DJ, Mitchell PO, Walp ER, Sutliff RL, Hart CM (2010) Rosiglitazone attenuates chronic hypoxia-induced pulmonary hypertension in a mouse model. Am J Respir Cell Mol Biol 42:482–490

Ota D, Kanayama M, Matsui Y, Ito K, Maeda N, Kutomi G, Hirata K, Torigoe T, Sato N, Takaoka A, Chambers AF, Morimoto J, Uede T (2014) Tumor-alpha9beta1 integrin-mediated signaling induces breast cancer growth and lymphatic metastasis via the recruitment of cancer-associated fibroblasts. J Mol Med (Berl) 92:1271–1281

Oyama Y, Akuzawa N, Nagai R, Kurabayashi M (2002) PPARgamma ligand inhibits osteopontin gene expression through interference with binding of nuclear factors to A/T-rich sequence in THP-1 cells. Circ Res 90:348–355

Palazzuoli A, Ruocco G, Cekorja B, Pellegrini M, Del Castillo G, Nuti R (2015) Combined BNP and echocardiographic assessment in interstitial lung disease for pulmonary hypertension detection. Int J Cardiol 178:34–36

Paulin R, Michelakis ED (2014) The metabolic theory of pulmonary arterial hypertension. Circ Res 115:148–164

Rabinovitch M (2008) Molecular pathogenesis of pulmonary arterial hypertension. J Clin Invest 118:2372–2379

Rabinovitch M, Guignabert C, Humbert M, Nicolls MR (2014) Inflammation and immunity in the pathogenesis of pulmonary arterial hypertension. Circ Res 115:165–175

Rangwala SM, Lazar MA (2004) Peroxisome proliferator-activated receptor gamma in diabetes and metabolism. Trends Pharmacol Sci 25:331–336

Ryan J, Dasgupta A, Huston J, Chen KH, Archer SL (2015) Mitochondrial dynamics in pulmonary arterial hypertension. J Mol Med (Berl) 93:229–242

Schermuly RT, Dony E, Ghofrani HA, Pullamsetti S, Savai R, Roth M, Sydykov A, Lai YJ, Weissmann N, Seeger W, Grimminger F (2005) Reversal of experimental pulmonary hypertension by PDGF inhibition. J Clin Invest 115:2811–2821

Stenmark KR, Meyrick B, Galie N, Mooi WJ, McMurtry IF (2009) Animal models of pulmonary arterial hypertension: the hope for etiological discovery and pharmacological cure. Am J Physiol Lung Cell Mol Physiol 297:L1013–L1032

Tachibana H, Ogawa D, Matsushita Y, Bruemmer D, Wada J, Teshigawara S, Eguchi J, Sato-Horiguchi C, Uchida HA, Shikata K, Makino H (2012) Activation of liver X receptor inhibits osteopontin and ameliorates diabetic nephropathy. J Am Soc Nephrol 23: 1835–1846

ten Freyhaus H, Dumitrescu D, Schnorbach S, Kappert K, Viethen T, Hellmich M, Hunzelmann N, Rosenkranz S (2015) CT-proET1 predicts pulmonary hemodynamics in scleroderma-associated pulmonary hypertension. Clin Res Cardiol 104:525–529

Walker LA, Walker JS, Glazier A, Brown DR, Stenmark KR, Buttrick PM (2011) Biochemical and myofilament responses of the right ventricle to severe pulmonary hypertension. Am J Physiol Heart Circ Physiol 301:H832–H840

Yuan JX, Rubin LJ (2005) Pathogenesis of pulmonary arterial hypertension: the need for multiple hits. Circulation 111:534–538

Zaitone SA, Barakat BM, Bilasy SE, Fawzy MS, Abdelaziz EZ, Farag NE (2015) Protective effect of boswellic acids versus pioglitazone in a rat model of diet-induced non-alcoholic fatty liver disease: influence on insulin resistance and energy expenditure. Naunyn Schmiedeberg's Arch Pharmacol 388:587–600